Influence of Secondary Precipitates and Crystallographic Orientation on the Strength of Single Crystals of a Ni-Based Superalloy

K. KAKEHI

The effect of crystallographic orientation and aging heat treatment at 850 °C on the creep rupture strength of single crystals of a nickel-based superalloy was examined at 700 °C in detail. Initial tensile orientations were selected over a wide range on the standard stereographic triangle. The $\{111\}\langle 112\rangle$–type slip systems were found to be operative during the creep deformation. The creep behavior was found to be greatly influenced by the additional aging at 850 °C for 20 hours. It was found that the effect of the aging at 850 °C was quite different between orientations favored for the $(\bar{1}11)[1\bar{1}2]$ slip system and those favored for the $(111)[\bar{2}11]$ slip system and that the creep deformation mechanisms of these two slip systems were different. In the orientations favored for $(\bar{1}11)[1\bar{1}2]$ slip systems, in the single-aged specimens, a small mean surface-to-surface spacing due to hyperfine γ' precipitates in the matrix channel promoted the $(\bar{1}11)[1\bar{1}2]$ slip and the primary creep. As a result of the additional aging at 850 °C, the hyperfine γ' precipitates were dissolved into the matrix, and the resultant large mean surface-to-surface spacing between the cuboidal precipitates inhibited extensive shearing of the γ-γ' structure by the $(\bar{1}11)[1\bar{1}2]$ slip system. As a result, the creep strengths of these orientations were increased in double-aged specimens; however, the low ductility associated with the difficulty of secondary noncoplanar slip did not enlarge rupture lifetime in the double-aged [001] specimen. In the orientations favored for the $(111)[\bar{2}11]$ slip system, creep deformation occurred by twinning shear through γ and γ' precipitates, and a distinct effect of the aging at 850 °C was not observed. In the multiple orientation of the $\{111\}\langle\bar{2}11\rangle$–type slip systems, *i.e.*, the $[\bar{1}12]$ and $[\bar{1}11]$ orientations, hyperfine precipitates improved creep strength because they prevented dislocations from gliding in the matrix channel in the single-aged specimens.

I. INTRODUCTION

THE anisotropy of the creep strength of single crystals of Ni-based superalloys has been interpreted in terms of the Schmid factors and multiplicity of $\{111\}\langle 112\rangle$–type slip systems in the intermediate-temperature ranges.[1,2] For the creep strength of a powder metallurgy RENÉ 95 alloy at 650 °C, the operative mechanism was essentially determined by the mean surface-to-surface spacing between the cooling γ' precipitates.[3] A small mean surface-to-surface spacing between γ' precipitates restricted dislocation motion significantly, whereas a larger mean surface-to-surface spacing between the γ' precipitates promoted homogeneous slip through a/2$\langle 110\rangle$ dislocation bowing and looping.[3] Secondary γ' precipitates in a matrix channel are expected to influence the mean surface-to-surface spacing between γ' precipitates. However, little attention has been paid to the effect of the secondary precipitates on the creep strength and activities of $\{111\}\langle 112\rangle$–type slip systems in the intermediate-temperature ranges. Therefore, the primary purpose of the present investigation is to study the effect of heat treatments on the secondary precipitates and to understand the resultant changes of creep behavior in each orientation. The second objective is to investigate the differences between $(\bar{1}11)[1\bar{1}2]$ and $(111)[\bar{2}11]$ slip systems.

K. KAKEHI, Research Associate, is with the Department of Mechanical Engineering, Tokyo Metropolitan University, Tokyo 192-0397, Japan.
Manuscript submitted October 23, 1997.

II. EXPERIMENTAL PROCEDURES

The investigation was carried out on an experimental nickel-based superalloy. Its chemical composition is listed in Table I. Single crystals of this alloy were grown from the melt by the modified Bridgman method. After the analysis of the crystallographic orientation by the back-reflection Laue method, specimens for creep rupture tests were cut from the as-grown crystals by a spark cutter. The specimens were solutionized at 1255 °C for 10 hours and then cooled in an air blast. Two kinds of procedures for the aging heat treatment were employed. The single-aged specimens were aged at 1100 °C for 10 hours, and the double-aged specimens were subjected to aging at 1100 °C for 10 hours and, subsequently, to an additional aging at 850 °C for 20 hours. After each aging treatment, the specimens were cooled in an air blast. Creep rupture tests were performed at 700 °C under a nominal stress of 820 MPa. The initial tensile orientations are shown in Figure 1. Dislocation structures were observed by transmission electron microscopy (TEM). The edge lengths of the γ' precipitates were measured by scanning electron microscopy (SEM).

III. EXPERIMENTAL RESULTS

A. *Microstructures of the Heat-Treated Specimens*

The distributions of the γ' precipitates after aging heat treatment are shown in Figure 2. The average edge lengths were 0.40 μm for the single-aged specimen and 0.39 μm for the double-aged specimen, respectively. The influence

Table I. **Chemical Composition of the Superalloy (Mass Percent)**

Cr	Mo	Co	W	Ta	Ti	Al	V	Ni
10.11	2.50	9.97	0.04	0.07	4.75	5.73	0.93	bal

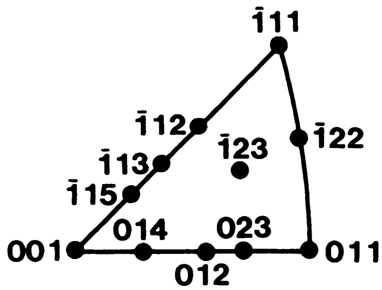

Fig. 1—Initial loading orientations.

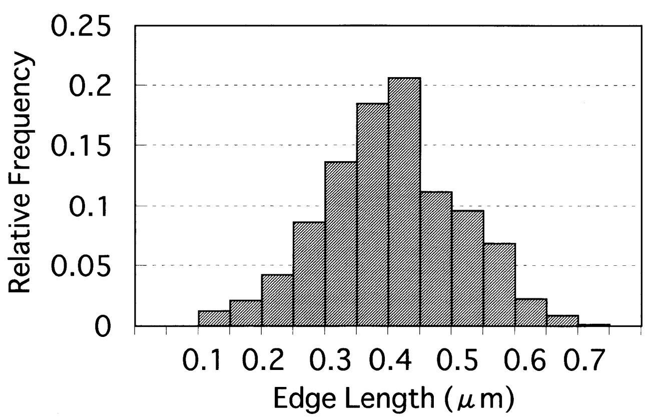

(*a*)

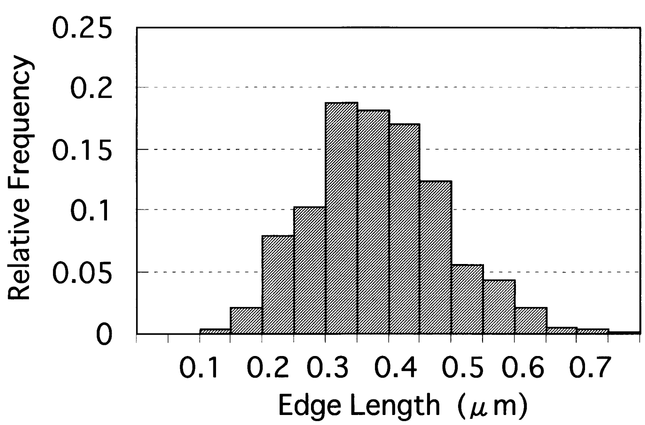

(*b*)

Fig. 2—The distribution of edge lengths of precipitates after aging heat treatment: (*a*) single aging and (*b*) double aging.

of the additional aging treatment at 850 °C on cuboidal γ' precipitates was not observable by SEM. The microstructures of heat-treated specimens were also observed by TEM. As shown in Figure 3, numerous hyperfine secondary γ' precipitates could be observed in the matrix channel for single aging; however, the hyperfine precipitates dissolved

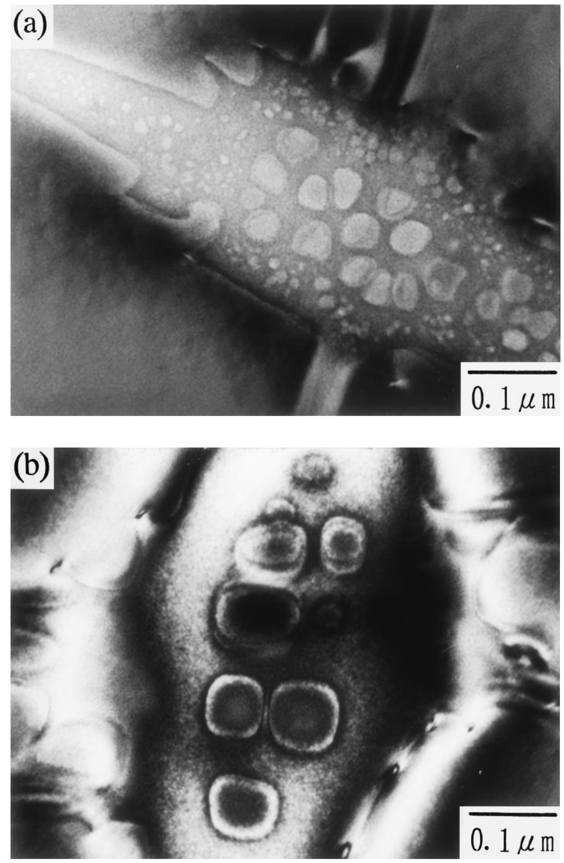

Fig. 3—Comparison of secondary γ' precipitates between (*a*) the single-aged specimen and (*b*) the double-aged specimen.

into the matrix and some of the precipitates coarsened after the aging at 850 °C.

B. *Effect of Crystallographic Orientation*

The results of the creep rupture test are shown in Figures 4 and 5. The lattice rotations of tensile direction due to creep deformation are illustrated in Figure 6. In the single-aged specimens (Figure 4), long rupture lifetimes occurred in the [001], $[\bar{1}12]$, and $[\bar{1}11]$ orientations. Compared to the [001] specimen, the specimens with the $[\bar{1}15]$ and $[\bar{1}13]$ orientations exhibited shorter lives. The tensile directions of these two specimens rotated toward $[1\bar{1}2]$ (Figure 6(a)) and actually failed during the first-stage creep. The creep curves of the [001], [014], and $[\bar{1}12]$ specimens included the steady-state region. The [012] specimen ruptured on loading because the creep testing stress exceeded its tensile strength. In the [011], $[\bar{1}22]$, [023], and $[\bar{1}23]$ orientations, the creep rupture lifetimes were very short and the rupture elongation was very large. The [011] and $[\bar{1}22]$ specimens rotated through a single-slip region of high Schmid factor toward $[\bar{2}11]$ (Figure 6(a)), but failed before reaching the [001]-$[\bar{1}11]$ intersecting boundary. From the lattice rotation analysis, $\{111\}\langle 112\rangle$–type slip systems were found to be operative during creeping.

Figure 5 shows the creep curves of the double-aged specimens. In the [001], $[\bar{1}15]$, $[\bar{1}13]$, [014], and [012] orientations, the creep curves showed a steady-state region. Long

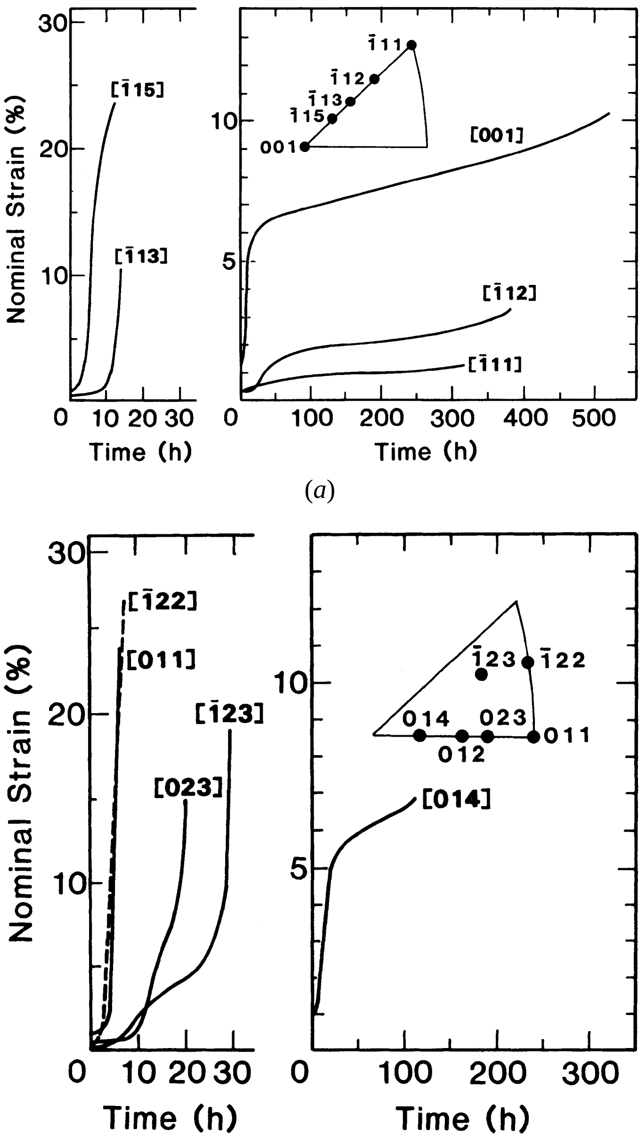

Fig. 4—Creep curves of the single-aged specimens: (*a*) orientations on the [001]-[$\bar{1}$11] boundary and (*b*) other orientations.

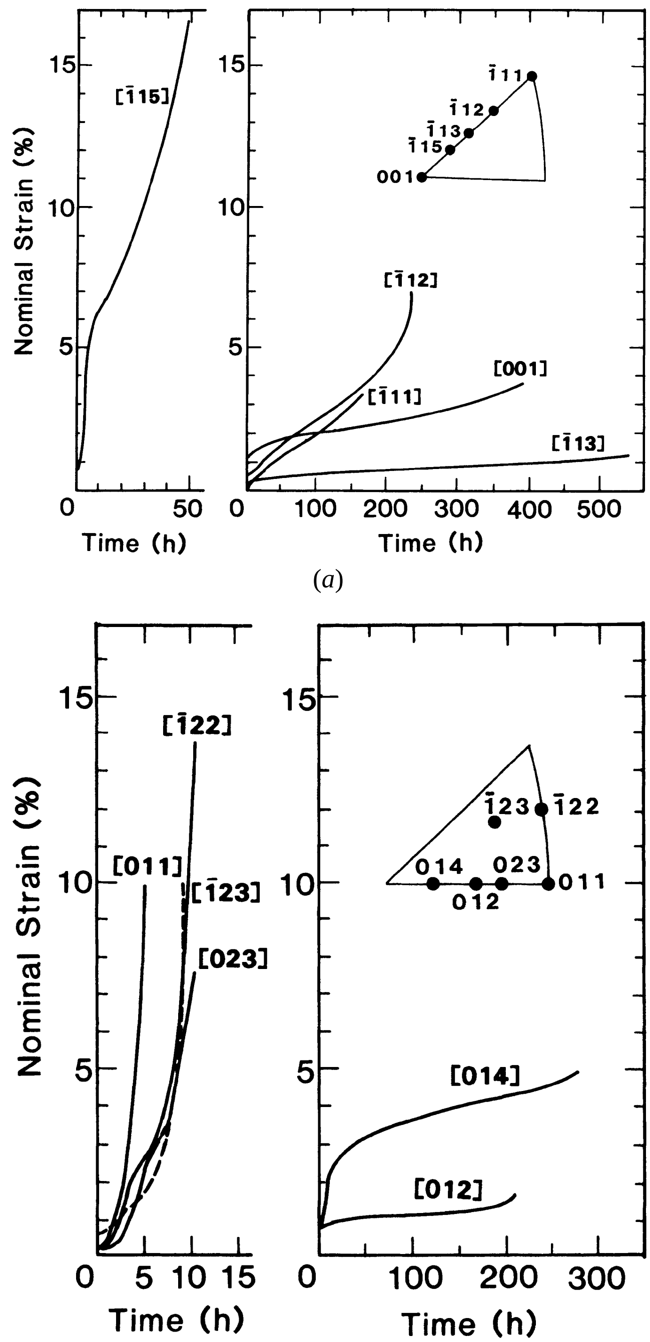

Fig. 5—Creep curves of the double-aged specimens: (*a*) orientations on the [001]-[$\bar{1}$11] boundary and (*b*) other orientations.

rupture lifetimes can be seen in the [001] and [$\bar{1}$13] orientations. Compared to the [001] and [$\bar{1}$13] specimens, the [$\bar{1}$15] specimen exhibited larger primary creep strain and shorter life, and its lattice rotated toward [$1\bar{1}2$] (Figure 6(b)). The [$\bar{1}$12] specimen rotated slightly toward [$\bar{1}$11]. This can be explained by the operation of a duplex slip of the (111)[$\bar{2}$11] and ($\bar{1}\bar{1}$1)[$\bar{1}$21] slip systems. The [011], [023], [$\bar{1}$22], and [$\bar{1}$23] orientations exhibited appreciably shorter lives and large rupture elongation because of the absence of strain hardening. The [011] and [$\bar{1}$22] specimens rotated through a single-slip region toward the [$\bar{2}$11] orientation (Figure 6(b)) and failed before reaching the [001]-[$\bar{1}$11] boundary.

C. *Effects of the Additional Aging at 850 °C*

The additional aging at 850 °C resulted in the remarkable change of the creep behavior in the [001], [$\bar{1}$15], [$\bar{1}$13], and [014] orientations. As shown in Figure 7(a), as a result of the aging at 850 °C, the primary creep strain in [001] reduced from 6.0 to 1.5 pct, and the minimum creep rate was also reduced. In spite of a decrease of the primary creep strain and minimum creep rate, the rupture lifetime of the specimen was decreased because the rupture elongation was reduced. As shown in Figure 8, fractures of both specimens occurred along the crystallographic planes, but the crystallographic planes were different. Fractures occurred along the ($\bar{1}$11) and ($1\bar{1}1$) planes in the single-aged specimen, whereas the planar fracture surface along a single (111) plane was observed in the double-aged specimen. The creep curves of the [$\bar{1}$15] and [$\bar{1}$13] orientations are shown in Figures 7(b)

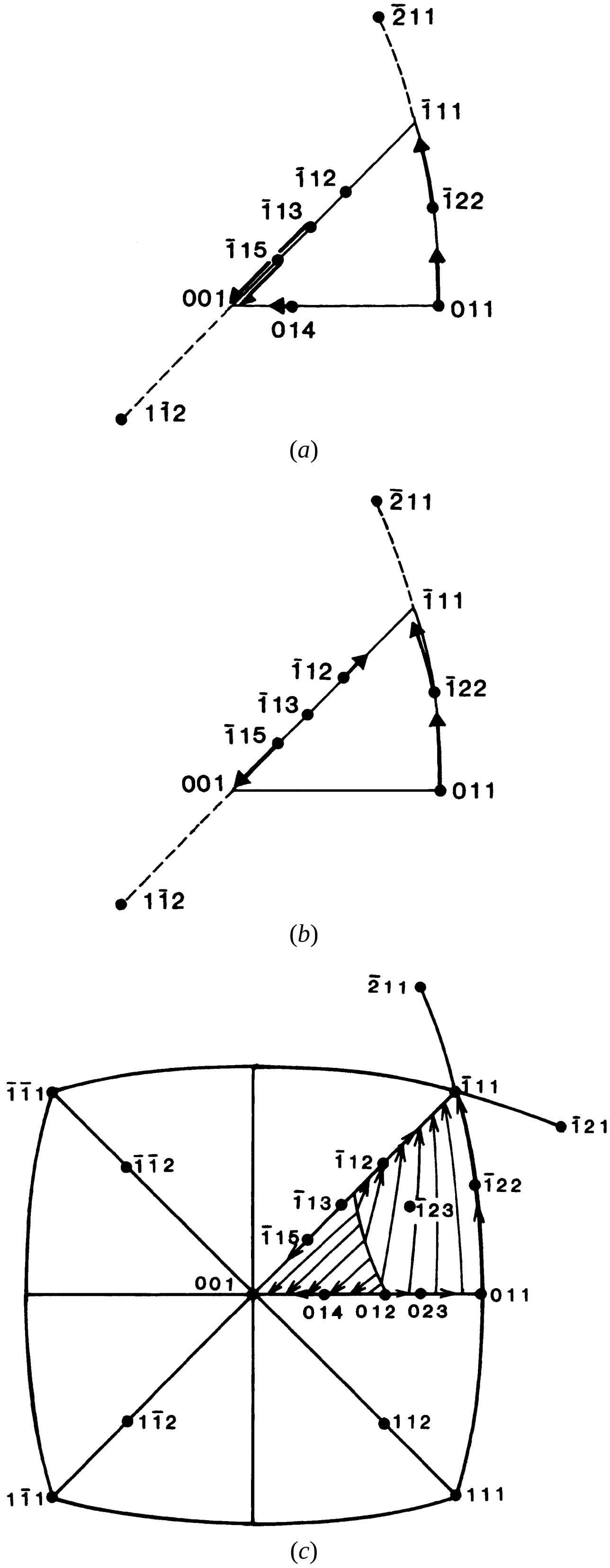

Fig. 6—Lattice rotations by creep deformation: (*a*) the single-aged specimens, (*b*) the double-aged specimens, and (*c*) {111}⟨112⟩ slip systems.

and (c), respectively. The single-aged specimen failed before the transition to the steady-state region due to the absence of strain hardening. On the other hand, the double-aged specimens showed both regions of primary and steady state, and their rupture lifetimes were significantly prolonged. The rupture lifetime of the [$\bar{1}13$] crystal increased by a factor of 40 (Figure 7(c)). Figure 9 shows the fracture surfaces of the [$\bar{1}13$] specimens. Fracture occurred along the ($\bar{1}11$), ($1\bar{1}1$), (111), and ($\bar{1}\bar{1}1$) planes in the single-aged specimen. However, (111) and ($\bar{1}\bar{1}1$) slip planes were observed in the double-aged specimen. In the [014] orientation, the primary creep strain also was reduced and its rupture lifetime increased (Figure 7(d)). In the [001], [115], [$\bar{1}13$], and [014] orientations, the additional aging at 850 °C brought about a remarkable decrease in rupture elongation. In contrast to these orientations, in the [$\bar{1}11$] and [$\bar{1}12$] orientations, as shown in Figure 10, the creep rates and rupture elongation increased and the rupture lifetimes decreased by the additional aging at 850 °C. However, in the [023], [$\bar{1}22$], [$\bar{1}23$], and [011] orientations, in spite of aging at 850 °C, the rupture lifetimes remained very short (Figure 5(b)). In the [011] and [023] orientations (Figure 11), the single-aged specimens showed an incubation period, but the incubation period disappeared in the specimens aged at 850 °C.

As shown in Figure 6(c), [001], [$\bar{1}15$], [$\bar{1}13$], and [014] orientations are favored for the ($\bar{1}11$)[$1\bar{1}2$] slip system ([001] and [014] are multiple orientations), and [023], [$\bar{1}22$], [$\bar{1}23$], and [011] orientations are favored for the (111)[$\bar{2}11$] slip system. The effect of the additional aging at 850 °C was different between the two orientation groups.

D. *Microstructural Observations by TEM after Creep*

In order to investigate the creep deformation mechanism, the microstructures of the crept specimens were observed by TEM. Figure 12 shows the microstructures after creep rupture in the double-aged [$\bar{1}15$] specimens. Individual precipitates were sheared by dislocations with the creation of superlattice stacking faults (Figure 12(a)). When the foil is cut along the (110) plane parallel to the stress axis, the stacking faults were found to be parallel to the ($\bar{1}11$) primary slip plane (Figure 12(b)).

The TEM microphotograph of the [011] specimen showed the microtwin lamellae that extend over both the γ and γ' phases (Figure 13) and the microtwins that had nucleated in the precipitates (Figure 14).

Figure 15 shows the crept TEM structure in the [$\bar{1}11$] orientation. Superlattice stacking faults and slip dislocations inside γ' precipitates were rare under both aging conditions. In the single-aged specimen, the density of the matrix dislocations was extremely low (Figure 15(a)) and the hyperfine precipitates remained undissolved after the creep test (Figure 15(b)), whereas dense interfacial dislocation networks were found to develop around the γ' precipitates after creep in the double-aged specimen (Figure 15(c)).

IV. DISCUSSIONS

A. *Influence of Additional Aging at 850 °C*

The additional aging at 850 °C resulted in remarkable changes in the creep behavior in each orientation, as described. A similar change in the [001] orientation was observed by Hopgood and Martin.[4] They tested single crystals of SRR99 close to the [001] orientation, at 750 °C under

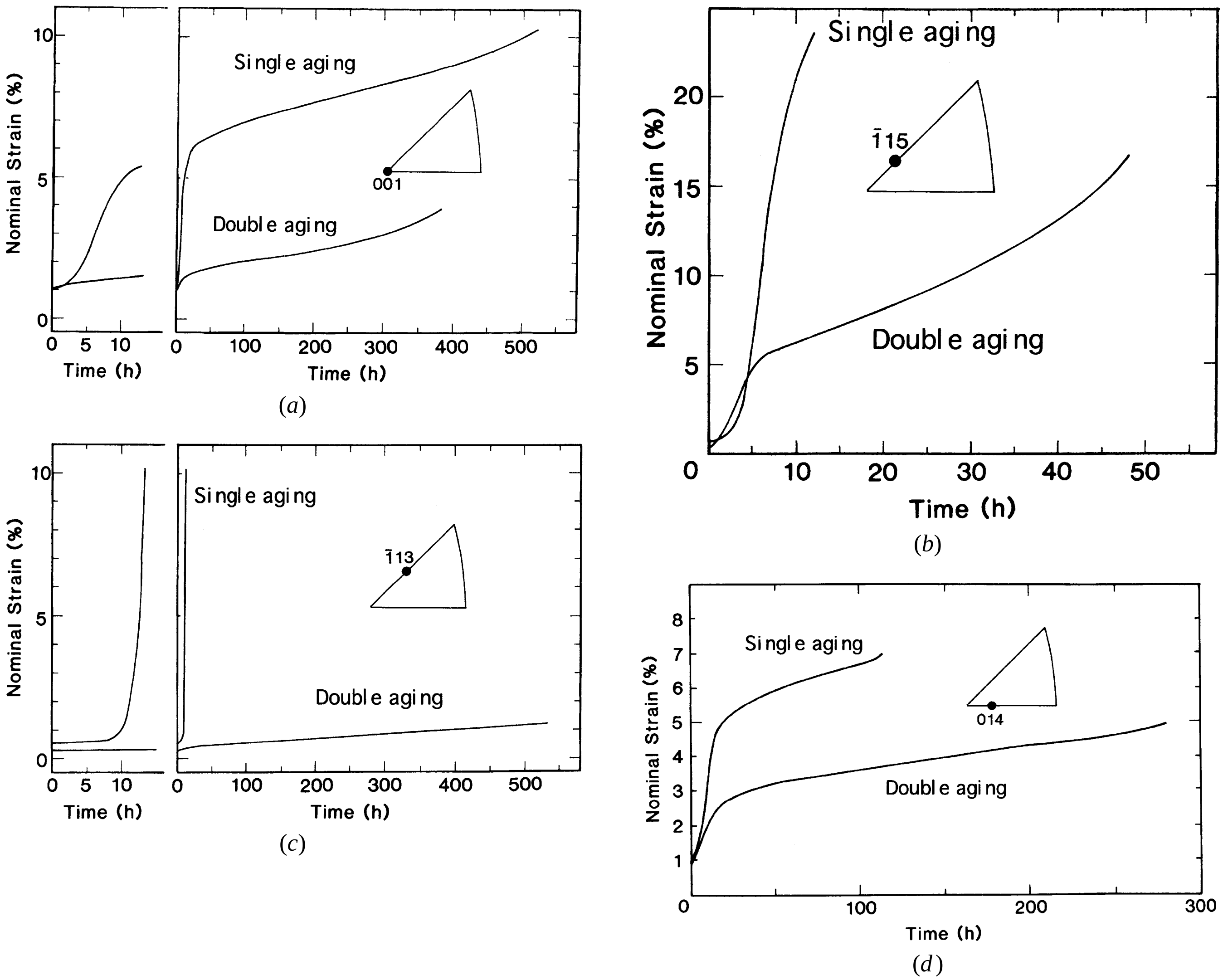

Fig. 7—Effect of aging heat treatment on creep behavior for each orientation: (*a*) [001], (*b*) [$\bar{1}$15], (*c*) [$\bar{1}$13], and (*d*) [014].

800 MPa. They reported that the primary creep stain was reduced by heat treatment at 870 °C for 16 hours prior to testing. Their atom probe analysis indicated that the heat treatment at 870 °C resulted in a build-up of chromium in the matrix close to the γ-γ' interfaces, and TEM observations showed an increase in the volume fraction of the γ' phase. They concluded that the solid-solution strength of Cr inhibited the shearing of precipitates by a/6$\langle 112 \rangle$ dislocations and, thus, decreased the extent of the primary creep deformation. However, in this study, the influence of aging at 850 °C is different in each orientation; therefore, it cannot be explained solely by the solid-solution strength of Cr at γ-γ' interfaces. In this study, a distribution of hyperfine secondary precipitates in the matrix channel was observed in the single-aged specimen (Figure 3(a)). Hopgood and Martin found that secondary γ' precipitation occurred after creep only in the single-aged specimen. The γ matrix is supersaturated for the specimens subjected to a single aging at high temperature, and the hyperfine secondary particles precipitate during cooling. The second aging at 850 °C caused these hyperfine precipitates to go back into solution and to reprecipitate as large precipitates. Extensive cooperative shearing of the γ-γ' structure by the $\{111\}\langle 112 \rangle$ slip, which promotes a large primary creep, predominates in the alloy containing the smallest precipitates.[5,6,7] A small mean surface-to-surface spacing between γ' precipitates promoted planar slip and shearing of the γ-γ' structure by $\{111\}\langle 112 \rangle$ slip, which was associated with the formation of complex faults within the γ' precipitates and also with stacking faults in the matrix, and the faults were on the common $\{111\}$ plane of the γ' and γ phase.[3] In orientations near [001] at an intermediate temperature, γ' precipitates were found to be sheared by pairs of a/2$\langle 112 \rangle$ dislocations, and intrinsic/extrinsic fault pairs were observed.[1,8–10] In the γ' precipitates, two a/2 $\langle 112 \rangle$ dislocations with the same Burgers vector split into three pairs of Shockley dislocations (super-Shockley dislocations[11]) having a unique Burgers vector and being separated by superlattice intrinsic/extrinsic stacking faults (S-ISF/S-ESF).[1,8–13] This is viscous slip in the $L1_2$-lattice precipitate[13] by the net Burgers vector of a$\langle 112 \rangle$. The dissociation of 2δC into two δC has been predicted by Paidar *et al.* in the so-called D1 core structure.[14] In this case, both partials are tightly linked by a shuffled planar core.[11] Courbon *et al.*[11] observed shearing processes of γ' and γ phases by super-Shockley dislocations *in situ* and revealed that a super-Shockley 2δC dislocation splits into two identical Shockley

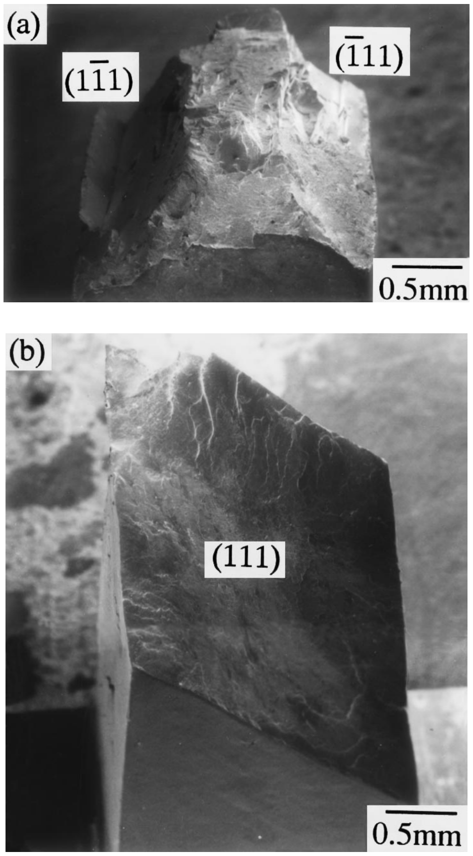

Fig. 8—Fracture surface of the [001] specimens showing crystallographic {111} facets of (*a*) the single-aged specimen (ε = 9.14 pct) and (*b*) the double-aged specimen (ε = 2.85 pct). Shear strains for the $(\bar{1}11)[1\bar{1}2]$ slip system are (a) 19.4 pct, and (b) 6.0 pct.

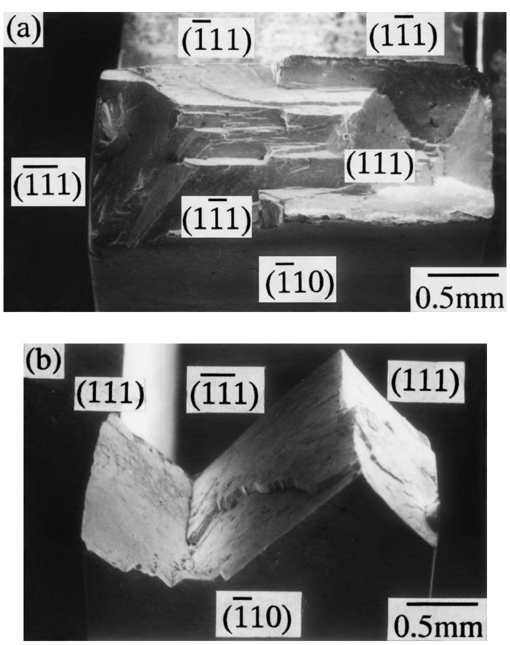

Fig. 9—Fracture surface of the $[\bar{1}13]$ specimens showing crystallographic {111} facets of (*a*) the single-aged specimen (ε = 22.61 pct) and (*b*) the double-aged specimen (ε = 2.0 pct). Shear strains for the $(\bar{1}11)[112]$ slip system are (a) 52.8 pct and (b) 4.7 pct.

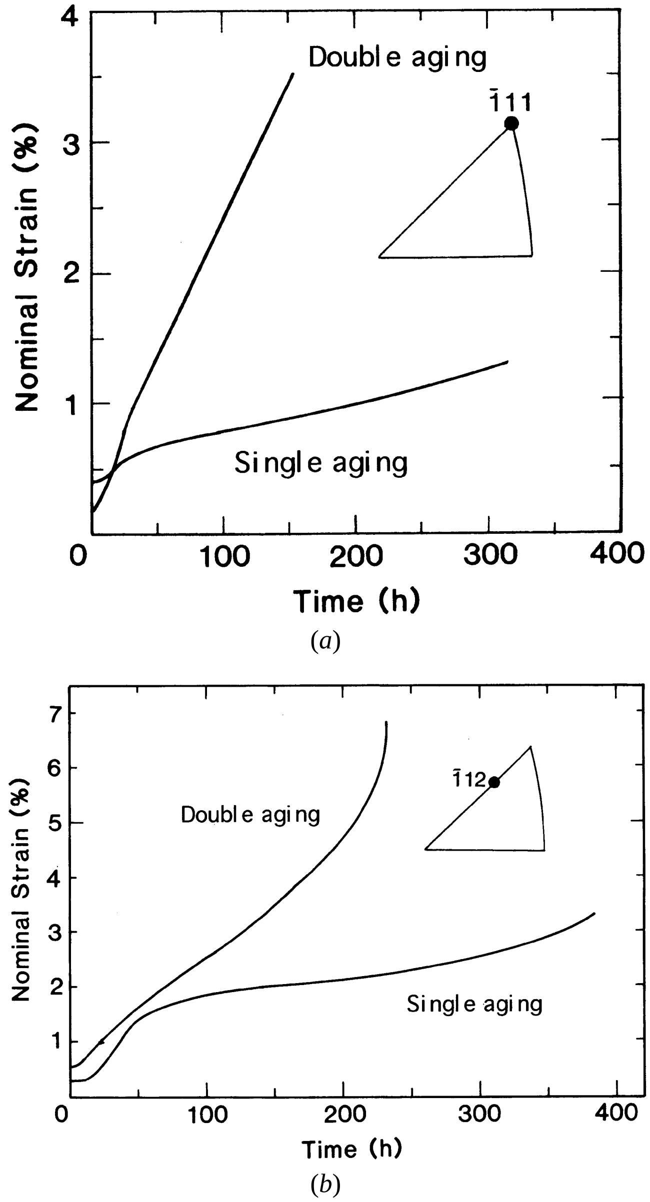

Fig. 10—Effect of aging treatment on creep behavior for each orientation: (*a*) $[\bar{1}11]$ and (*b*) $[\bar{1}12]$.

δC dislocations on two adjacent close-packed planes in the γ phase, and that these would shear the γ channel separately. When the surface-to-surface spacing between precipitates is small, the dislocations would shear both γ' and γ phases successively, keeping the dissociated dislocation structure within the γ' precipitate. In the case of the large surface-to-surface spacing between precipitates, the dissociated dislocations in the precipitates have to recombine into the matrix dislocations to shear the matrix channel. Therefore, the small spacing of the matrix channel will promote the extensive cooperative shearing of γ-γ' structure by the $\{111\}\langle 112\rangle$ slip. The average edge lengths of cuboidal primary precipitates were 0.40 μm for the single-aged specimen and 0.39 μm for the double-aged specimen. Secondary γ' precipitation did not significantly change the edge length of the cuboidal primary precipitates; however, it can measurably decrease the net width of these matrix channels. Therefore, in the single-aged specimen, the $\{111\}\langle 112\rangle$ slip would

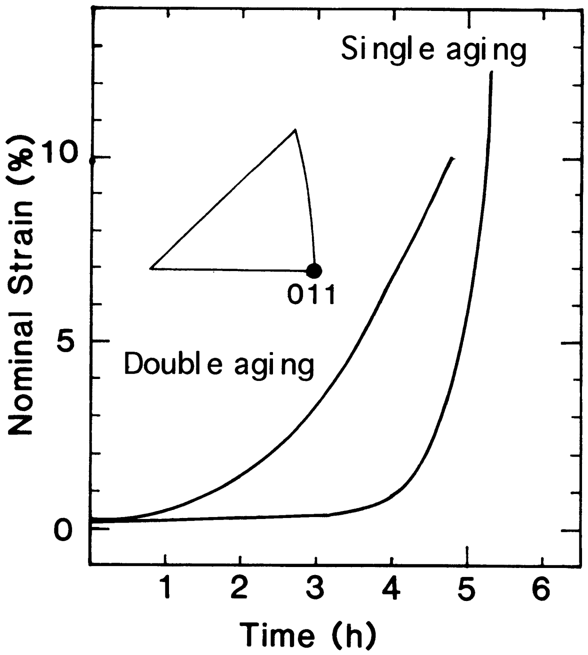

(*a*)

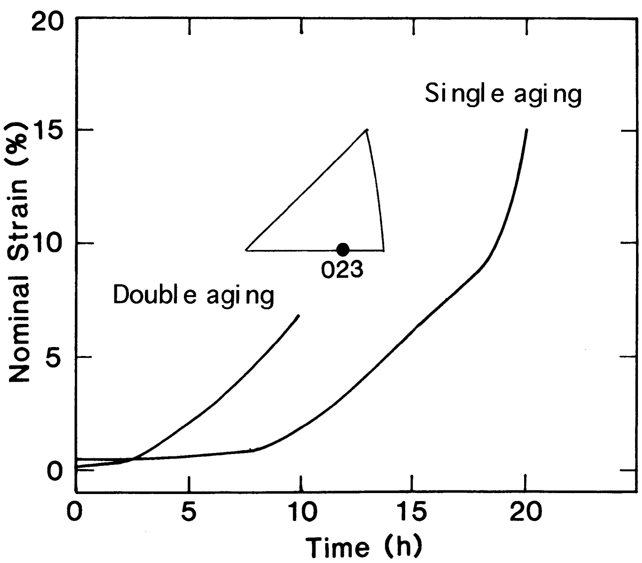

(*b*)

Fig. 11—Effect of aging treatment on creep behavior for each orientation: (*a*) [011] and (*b*) [023].

be promoted because of a small mean surface-to-surface spacing between hyperfine secondary precipitates. Since the aging at 850°C resulted in the solution of hyperfine precipitates (Figure 3(b)) in the double-aged specimen, the extensive and cooperative shearing of the γ-γ' structure by the {111}⟨112⟩ slip would be prohibited because of large interspacing between cuboidal primary precipitates. In the case of the [001] specimen of the CMSX2 alloy containing the large γ' precipitates, the precipitates were sheared individually by the {111}⟨112⟩ slip and stacking faults were confined primarily to the individual precipitates.[6] This suggests that an extended matrix channel inhibits extensive and cooperative shearing of the γ-γ' structure.

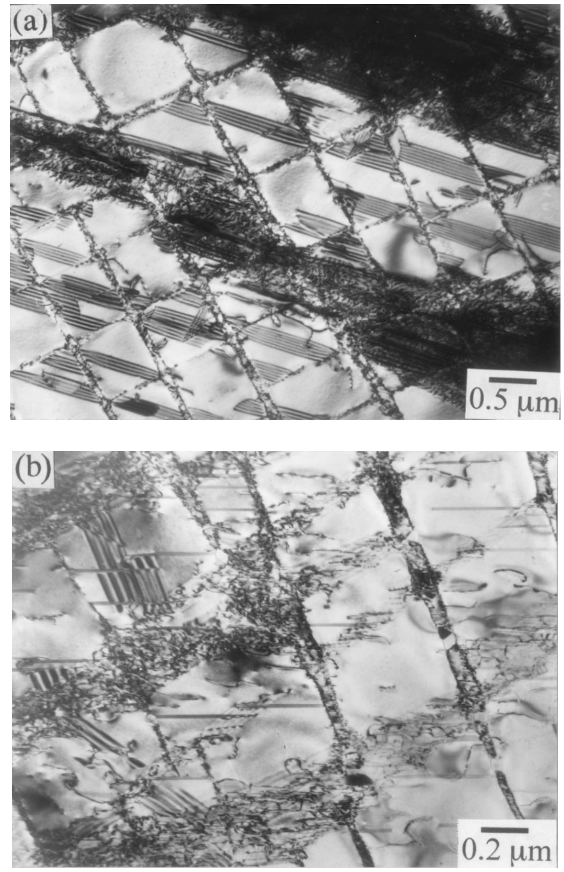

Fig. 12—Dislocation structures of the double-aged specimens in the [$\bar{1}$15] orientation (ε = 10.0 pct). (*a*) The foil normal is [001]: *g*//[200]. Shear strains for the ($\bar{1}$11)[1$\bar{1}$2] slip system are 20.5 pct. (*b*) When the foil is cut along the (011) plane of specimen, it is found that stacking faults are on the ($\bar{1}$11) plane in the γ' precipitates: *g*//[111].

However, the hyperfine secondary precipitates would prohibit a/2⟨110⟩ dislocations from gliding in the matrix channel. Since a larger mean surface-to-surface spacing between the γ' precipitate promotes homogeneous slip through 1/2⟨110⟩ dislocation bowing and looping in the matrix,[3] the solution of hyperfine precipitates into the matrix increases the net channel width and promotes the dislocation glide in the matrix channel. The a/2⟨110⟩ dislocation motion in the matrix channel leaves interfacial dislocations around cuboidal precipitates during the incubation period[15,16] and forms the homogeneous γ-γ' interfacial dislocation networks.[15–20] The loss of coherency of the γ-γ' interface might prohibit partial dislocations from shearing cuboidal precipitates. Link and Feller–Kniepmeier[15] have shown that the shearing of γ' precipitates by the {111}⟨112⟩ slip requires coherent interfaces, because (1) coherency stresses allow the energetically favorable deposition of a/6⟨112⟩ dislocation in the interface, and (2) dislocation networks in the interface inhibit the partial dislocation from entering into γ' precipitates and the propagation of the triple dislocation node. The formation of interfacial dislocation networks destroys these conditions.

In conclusion, in the [001], [$\bar{1}$15], [$\bar{1}$13], and [014] orientations, as shown in Figures 7(a) through (d), we can be fairly certain that a small mean surface-to-surface spacing between hyperfine secondary precipitates promotes primary creep, which is associated with the activity of the ($\bar{1}$11)[1$\bar{1}$2] slip

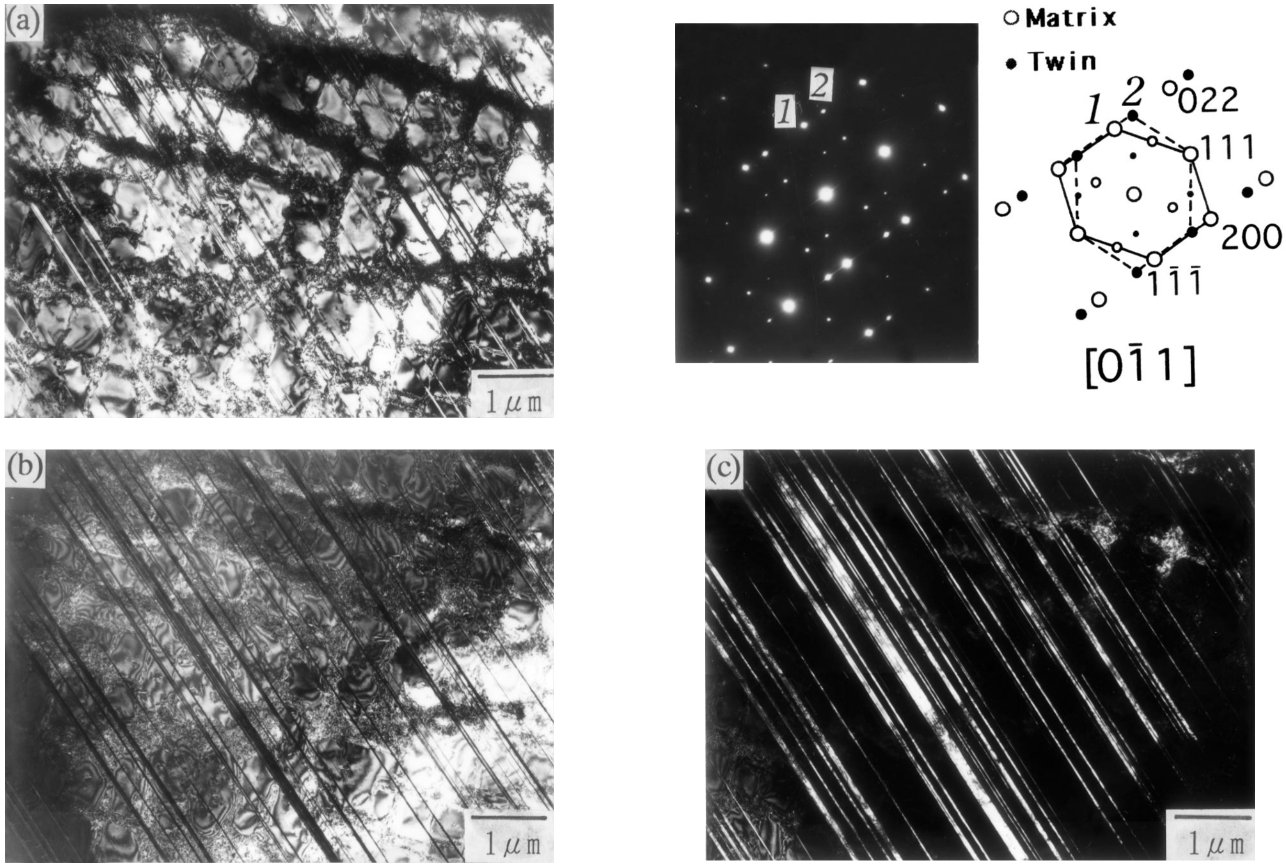

Fig. 13—TEM micrographs of the ruptured [011] specimen showing microtwin lamellae (ε = 9.6 pct). The foil normal is $[0\bar{1}1]$. (*a*) Bright-field micrograph. (*b*) Dark-field micrograph using spot *1*. (*c*) Dark-field micrograph using spot *2*. Shear strain for the $(111)[\bar{2}11]$ slip system is 20.4 pct.

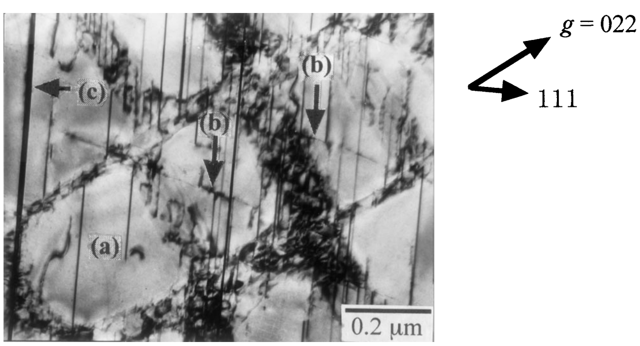

Fig. 14.—TEM micrograph showing the nucleation of mechanical microtwins. The same thin foil of Fig. 13 was observed. It was observed that (*a*) microtwins were nucleated in the precipitates and (*b*) twin dislocations rotated around their poles in the precipitates. (*c*) Thin twin lamellae extend through both γ and γ' phases.

system, and that the large mean surface-to-surface spacing between cuboidal precipitates and the γ-γ' interfacial dislocation networks inhibits the partial dislocations from shearing the precipitates and suppresses primary creep.

In the [001] orientation, in spite of the remarkable decrease of the primary creep strain in the double-aged specimen, the rupture lifetime of the specimen was not increased (Figure 7(a)). Fractures occurred along the $(\bar{1}11)$ and $(1\bar{1}1)$ planes in the single-aged specimen, whereas the fracture surface along a single (111) slip plane was observed in the double-aged specimen (Figure 8). It was also observed that the planar fracture surface parallel to (111) resulted in low rupture elongation and short rupture life.[7] The secondary slip, with a shear displacement component perpendicular to the crack plane, can relax the normal stress of the primary slip; therefore, the difficulty of activating secondary slip in return results in large hydrostatic and normal stresses near the crack tip.[21] The combination of intense coplanar shear and large normal stresses results in easy crack propagation and low toughness.[21] In the double-aged specimen, the slip deformation on the {111} plane was inhibited because of the interfacial dislocation network. However, at some point during creep deformation, once the local slip on {111} has accidentally occurred by a stress concentration at the microstructural defects (*e.g.*, micropores and surface defects), this stress concentration would not be relaxed because the secondary noncoplanar slip is difficult to operate. The low ductility associated with the difficulty of secondary noncoplanar slip might not enlarge rupture lifetime in the double-aged [001] specimen.

The creep rate and rupture elongation in the $[\bar{1}11]$ orientation were increased by the additional aging at 850 °C (Figure 10(a)), in contrast to the case of the [001], $[\bar{1}15]$, $[\bar{1}13]$, and [014] orientations. However, in the creep of the $[\bar{1}11]$ specimens, it is difficult for the dislocations to shear the γ' precipitates because of the low Schmid factor for slip systems on {111} planes (Table II). Hence, Orowan bypassing, which leads to a homogeneous deformation structure in the matrix, would come into operation.[7] As mentioned previously, the second aging dissolved the hyperfine precipitates

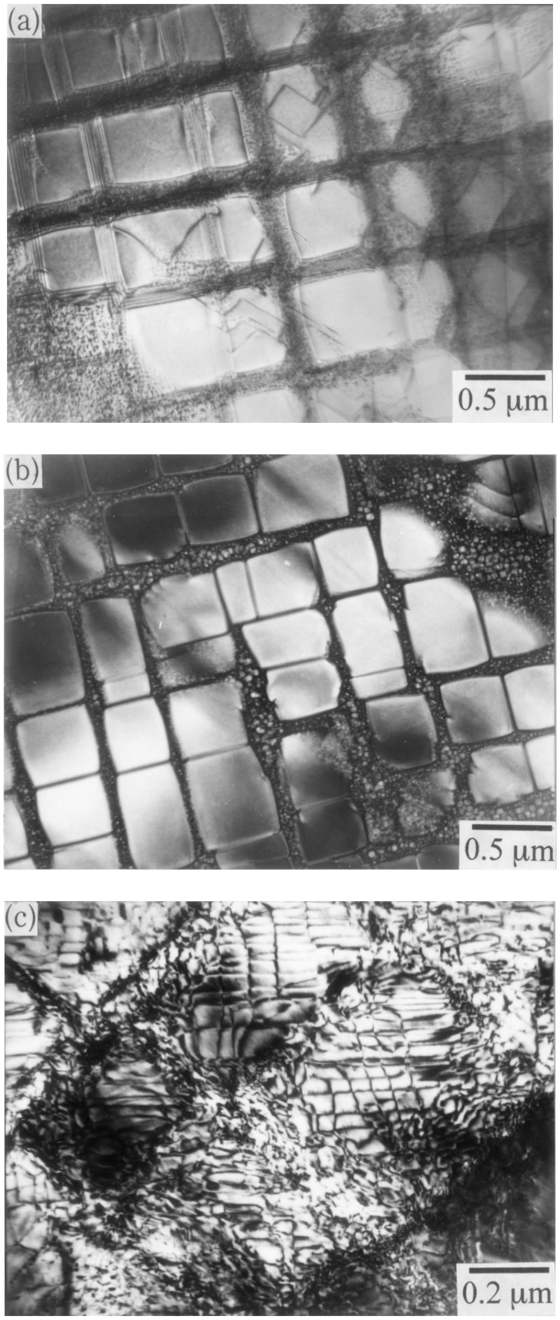

Fig. 15—Interfacial dislocations of the crept $[\bar{1}11]$ specimens: (*a*) and (*b*) single aged and (*c*) double aged. The thin foils were cut from the same specimens as shown in Fig. 14. The foil normal was cut along the (001) plane to observe the interfacial dislocations. Shear strains for the $\{100\}\langle 011\rangle$ slip system are (*a*) and (*b*) 2.8 pct, and (*c*) 7.4 pct.

Table II. Schmid Factors for Slip Systems

Orientation	$(111)[\bar{1}01]$	$(\bar{1}11)[1\bar{1}2]$	$(111)[\bar{2}11]$
[001]	0.4082	0.4714	0.2357
$[\bar{1}15]$	0.4536	0.4886	0.3492
$[\bar{1}13]$	0.4454	0.4285	0.3857
$[\bar{1}12]$	0.4082	0.3771	0.3928
$[\bar{1}11]$	0.2722	0.0000	0.3143
[014]	0.4803	0.4853	0.3466
[012]	0.4899	0.4243	0.4243
[023]	0.4711	0.3626	0.4533
[011]	0.4082	0.2357	0.4714
$[\bar{1}22]$	0.4082	0.1039	0.4714
[123]	0.4666	0.3030	0.4714

into the matrix, and the net width of the matrix was increased. In the $[\bar{1}11]$ orientation, cube slip of the screw dislocation segments was found, and this cube slip on the γ-γ' interface is facilitated by the high value of the Schmid factor of 0.4714 for the $\{100\}\langle 110\rangle$ slip system and the highly regular alignment of the γ' precipitates.[22] Screw dislocations might overcome obstacles by repeated cross-slip on two {111} planes.[22,23] In either case, the creep deformation of the $[\bar{1}11]$ specimens occurred mainly in the matrix phase. Furthermore, for the high symmetry of matrix arrangement, all three types of matrix channels are equally highly stressed, and strain hardening is poor despite the operation of multiple slip systems, because the probability of dislocation interaction is low in the matrix.[22] The deformation operated mainly by coplanar slip in the primary slip plane (111) along the $[\bar{1}10]$ and $[\bar{1}01]$ directions, and this deformation mode causes only a weak strain hardening, which results in the high creep rate.[24] As a result of these, the matrix dislocations glided easily in the matrix channel, dislocation networks developed along the γ-γ' interface (Figure 15(c)), and the creep rate was increased in the double-aged specimen. In the single-aged specimen, hyperfine secondary precipitates prevent the dislocation motion in the matrix channel, which would result in an extremely low creep rate.

B. *Transition from Primary Creep to Steady-State Creep*

MacKay and Maier concluded that second-stage creep deformation begins only after the occurrence of sufficient strain hardening, because of the interaction of $\{111\}\langle 112\rangle$–type slip systems.[2] However, the single-aged [001] specimen showed extensive primary creep strain in spite of being on a multiple-slip orientation (Figure 7(a)). Furthermore, the $[\bar{1}15]$ specimen requires about 13 pct tensile strain in order to reach the [001] multiple-slip orientation; however, in the double-aged specimen (Figure 7(b)), only half the amount of strain was observed when second-stage creep deformation began. Therefore, it is likely that second-stage creep deformation will begin when γ-γ' interfacial dislocation networks build up, which inhibit the partial dislocations from shearing the precipitates.

C. *Differences between $(\bar{1}11)[1\bar{1}2]$ Slip and $(111)[\bar{2}11]$ Slip*

As mentioned in Section III–B, the effect of the additional aging at 850 °C was quite different between the orientations favored for the $(\bar{1}11)[1\bar{1}2]$ slip system and those favored for the $(111)[\bar{2}11]$ slip system. In spite of the additional aging at 850 °C, the rupture lifetimes in the [023], $[\bar{1}22]$, $[\bar{1}23]$, and [011] orientations remained very short (Figure 5(b)). A comparison between Figures 12(b) and 13 shows a striking difference in terms of their overall deformation. The TEM photomicrograph of the [011] specimen shows the microtwin lamellae that extend over both the γ and γ' phases (Figure 13); however, microtwin lamellae were not observed in the $[\bar{1}15]$ specimen (Figure 12(b)). Mechanical twins are usually produced in bcc or hcp metals under conditions of a rapid rate of loading (shock loading) and decreased temperature. Face-centered cubic metals are not ordinarily considered to deform by mechanical twinning, except for rare cases.[25] Twinning is not a dominant deformation mechanism in metals which possess many possible slip systems, and it generally occurs when the slip systems are restricted or when something increases the critical resolved shear stress so that the twinning stress is less than the stress for slip.[25] The yield stress of γ' precipitates increases with increasing temperature, up to a peak temperature of 650 °C to 800 °C.[26,27] Since the critical stress for twinning will be lower than that for the slip near the peak temperature, novel mechanical twins would occur in the Ni superalloy. Kear[10] suggested the nucleation model of twinning in a Ni-based superalloy. In orientations near [011], there is a greater tendency of γ' precipitate shearing by the motion of single a/2$\langle 112 \rangle$ dislocations, rather than as pairs of such dislocations near the [001] orientation. Since a/2$\langle 112 \rangle \rightarrow$ a/3$\langle 112 \rangle$ + a/6$\langle 112 \rangle$, each γ' precipitate was sheared by an a/3$\langle 112 \rangle$ superlattice partial with the fault (S-ISF or S-ESF fault, depending on the sense of dislocation motion) bounded by an a/6$\langle 112 \rangle$ Shockley partial; the latter is unable to pass through the γ' precipitate easily because it creates a high-energy fault. Accumulation of such stacking faults by successive shear in neighboring slip planes leads to a situation where energy minimization favors the formation of new faults alongside existing ones, resulting in the nucleation of thin twins in the γ' phase. Microtwins are, thus, nucleated in the precipitates.[28] The ordered structure of the precipitates was preserved by twinning (Figure 13). If an a/6$\langle 112 \rangle$ Shockley dislocation shears the γ' precipitates, the $L1_2$ ordered structure will be destroyed. Therefore, an a/3$\langle 112 \rangle$ super-Shockley dislocation would be repeated on every {111} plane through a simple polar mechanism in the precipitate.[28] The microtwins in the precipitates will coalesce beyond a critical size.[28] The bounding Shockley partials at the γ-γ' interfaces build up internal stresses, and, at some point, these stresses are relieved by the propagation of the twins through the γ phase as groups of neighboring γ-γ' interface dislocations of opposite sign undergo mutual annihilation.[10] This leads to a reversed strain in the matrix, but which is energetically favorable, and to a strong anchor line for the trailing δA which is pinned, and twinning will then proceed with 2δA alone and may extend to the matrix with the help of the Suzuki effect.[28] The alloying elements that partition preferentially to the γ matrix,[29] *e.g.*, Co, Mo, and, particularly, Cr, are known to reduce the stacking fault energy (SFE) of nickel.[30,31,32] The SFE in superalloys can be reduced from 40 to more than 80 pct compared to that of pure Ni.[32] The low stacking energy of the matrix can result in twinning in the Ni superalloy. Compared to commercial alloys, the alloy used in this study contains a higher total concentration of Co, Mo, and Cr. A lower SFE in the matrix may be the reason why extensive twinning was observed in this alloy.

The final result of the process is the creation of thin twin lamellae that extend through both the γ and γ' phases, as shown in Figure 13. The twin dislocation rotates around its pole on every successive {111} plane.[28] By such a mechanism, a twin can propagate very quickly in the absence of diffusion and is not subjected to the need for a separate partial dislocation source on every (111) plane.[33] Therefore, the nucleation of the twin must be a rate-determining step rather than the propagation process. Since microtwins are nucleated in the primary precipitates, the hyperfine secondary precipitates in the matrix would not significantly affect the rupture lifetime of the [011] specimen (Figure 11(a)). However, on comparing the creep curves in detail, the differences between single- and double-aged specimens were observed. The single-aged specimen showed an incubation period, but the incubation period disappeared in the double-aged specimen. An incubation period has been observed in the creep of single-crystal Ni-based superalloys.[1,10,16,34] This incubation period is most likely due to the low initial dislocation density.[10] In Cu single crystals, it was indicated that previous deformation was necessary to form twins.[35] These results show that the formation of twins requires dislocations. The interaction between two matrix dislocations with perpendicular Burgers vectors of a/2[110] and a/2[$1\bar{1}0$] will create the superlattice twin dislocation 2δA and a strong anchor line, and the twin dislocation rotates around its pole dislocation with a Burgers vector of a/2[110].[28] The hyperfine secondary precipitates would retard the twin nucleation by preventing the dislocations from gliding in the matrix channel, which resulted in an incubation period in the single-aged specimen. However, during the incubation period, the matrix dislocations will gradually glide in the matrix channel, bypassing the hyperfine precipitates. For the superlattice twin dislocation 2δA, it would be more difficult to move in the matrix than in the precipitates because it requires the help of the Suzuki effect to move in the matrix.[28] Consequently, the small matrix spacing promotes the twin propagation; therefore, the tertiary creep rate for the single-aged specimen was larger than that for the double-aged specimen.

The twinning shear is always directional in the sense that the shear in one direction is not equivalent to the shear in the opposite direction. Twinning in fcc metals occurs on {111} planes in $\langle 112 \rangle$ directions. The atomic movements by twinning are illustrated in Figure 16.[33] Label *E* shows the atomic position after the occurrence of twinning deformation. The shaded atom A can move easily in the [$\bar{1}1\bar{2}$] direction, but atom J is hindered from moving in the [$1\bar{1}2$] direction by the top face of atom B. In the tensile creep of the [011] orientation, twinning occurs by the shear on the (111) plane in the [$\bar{2}11$] direction but not by the shear in the opposite direction. The [$\bar{1}15$] orientation has a larger Schmid factor for the {$\bar{1}11$}$\langle 1\bar{1}2 \rangle$ slip system than the [001] orientation (Table II) and is an easy glide orientation for the slip system (Figure 6(c)). The microtwin lamellae could not be observed (Figure 12), because the direction of the applied shear stress on the (111) plane is opposite that of twinning. Since it is impossible to form twins, another deformation mechanism comes into operation. As mentioned in Section IV–A, in orientations near [001], γ' precipitates are sheared by a pair of S-ISFs/S-ESFs. Since the extended matrix channel would be an obstacle for this shearing process, the secondary hyperfine precipitates significantly affected creep strength. The differences between the creep deformation mechanisms must be the reason why the influence

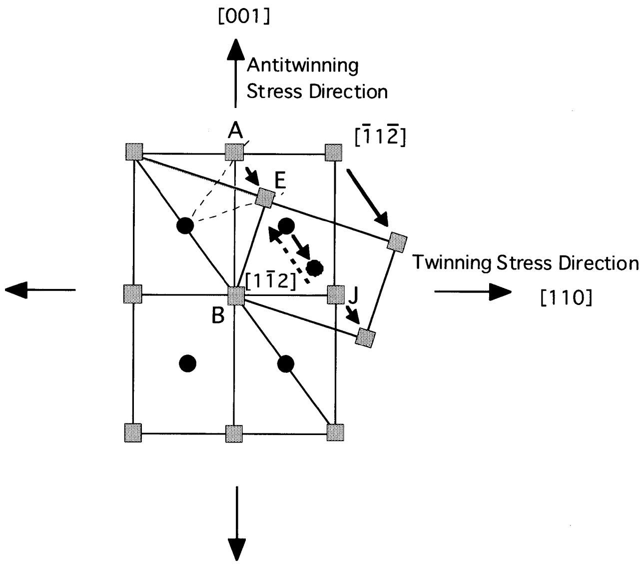

Fig. 16—Plan view of the (110) plane in the fcc crystal lattice showing the upper right half of the lattice twinned on the $(\bar{1}11)$ $[\bar{1}1\bar{2}]$ system. The atoms in the (110) plane layer are shown as squares, while the atoms under the atomic layer are indicated by circles.

of the additional aging at 850 °C was quite different between orientations favored for the $(\bar{1}11)[1\bar{1}2]$ slip system and those favored for the $(111)[\bar{2}11]$ slip system.

V. CONCLUSIONS

In the intermediate-temperature range, the creep behavior was found to be greatly influenced by the additional aging at 850 °C for 20 hours. From lattice rotation analysis, $\{111\}\langle 112\rangle$–type slip systems were found to be operative during creep at 700 °C in this nickel-based superalloy. The effect of aging at 850 °C was quite different between orientations favored for the $(\bar{1}11)[1\bar{1}2]$ slip system and those favored for the $(111)[\bar{2}11]$ slip system.

In the orientations favored for $(\bar{1}11)[1\bar{1}2]$ slip systems, a small mean surface-to-surface spacing due to hyperfine γ' precipitates in the matrix channel promoted the $(\bar{1}11)[1\bar{1}2]$ slip and primary creep in the single-aged specimen. As a result of the additional aging at 850 °C, the creep strength was increased because the large mean surface-to-surface spacing inhibited the activity of $(\bar{1}11)[1\bar{1}2]$–type slip systems, and the rupture elongation of these orientations was decreased because of low ductility associated with the difficulty of secondary noncoplanar slip.

In the [023], $[\bar{1}22]$, $[\bar{1}23]$, and [011] orientations favored for the $(111)[\bar{2}11]$ slip system, when the specimens were aged at 850 °C, the rupture lifetimes remained very short and the incubation period of creep strain disappeared. It was found that creep deformation occurred by twinning shear through γ and γ' phases.

In the $[\bar{1}11]$ and $[\bar{1}12]$ orientations, the hyperfine precipitates led to improvement of creep strength because they prevented dislocations from gliding in the matrix channel in the single-aged specimens.

REFERENCES

1. G.R. Leverant and B.H. Kear: *Metall. Trans.*, 1970, vol. 1, pp. 491-98.
2. R.A. MacKay and R.D. Maier: *Metall. Trans. A*, 1982, vol. 13A, pp. 1747-54.
3. P.R. Bhowal, E.F. Wright, and E.L. Raymond: *Metall. Trans. A*, 1990, vol. 21 A, pp. 1709-17.
4. A.A. Hopgood and J.W. Martin: *Mater. Sci. Eng.*, 1986, vol. 82, pp. 27-36.
5. P. Caron and T. Khan: *Strength of Metals and Alloys*, Pergamon Press, Elmsford, NY, 1989, pp. 893-98.
6. T. Khan and P. Caron: *Mater. Sci. Technol.*, 1986, vol. 2, pp. 486-92.
7. P. Caron, Y. Ohta, Y.G. Nakagawa, and T. Khan: in *Superalloys 1988*, D.N. Duhl, G. Maurer, S. Antolovich, C. Lund, and S. Reichman, eds., TMS, Warrendale, PA, 1988, pp. 215-24.
8. B.H. Kear, G.R. Leverant, and J.M. Oblak: *Trans. ASM*, 1969, vol. 62, pp. 639-50.
9. B.H. Kear, J.M. Oblack, and A.F. Giamei: *Metall. Trans.*, 1970, vol. 1, pp. 2477-86.
10. B.H. Kear: in *Order-Disorder Transformations in Alloys*, H. Warlimont, ed., Springer-Verlag, New York, NY, 1974, pp. 440-74.
11. J. Courbon, F. Louchet, M. Ignat, J. Pélissier, and P. Debrenne: *Phil. Mag. Lett.*, 1991, vol. 63, pp.73-78.
12. B.H. Kear, A.F. Giamei, G.R. Leverant, and J.M. Oblack: *Scripta Metall.*, 1969, vol. 3, pp. 123-30.
13. B.H. Kear, A.F. Giamei, G.R. Leverant, and J.M. Oblack: *Scripta Metall.*, 1969, vol. 3, pp. 455-60.
14. V. Paidar, M. Yamaguchi, D.P. Pope, and V. Vitek: *Phil. Mag.*, 1982, vol. 45, pp. 883-94.
15. T. Link and M. Feller-Kniepmeier: *Metall. Trans. A.*, 1992, vol. 23A, pp. 99-105.
16. T.M. Pollock and A.S. Argon: *Acta Metall. Mater.*, 1992, vol. 40, pp. 1-30.
17. A.K. Singh, N. Louat, and K. Sasanada: *Metall. Trans. A*, 1988, vol. 19A, pp. 2965-73.
18. T.P. Gabb, S.L. Draper, D.R. Hull, R.A. MacKay, and M.V. Nathal: *Mater. Sci. Eng.*, 1989, vol. A118, pp. 59-69.
19. R.D. Field, T.M. Pollock, and W.H. Murphy: in *Superalloys 1992*, S.D. Antolovich, R.W. Stusrud, R.A. MacKay, D.L. Anton, T. Khan, R.D. Kissinger, and D.L. Klarstrom, eds., TMS, Warrendale, PA, 1992, pp. 557-66
20. A. Lasalmonie and J.L. Strudel: *Phil. Mag.*, 1975, vol. 32, pp. 937-49
21. D.A. Koss and K.S. Chan: *Acta Metall.*, 1980, vol. 28, pp. 1245-52.
22. V. Sass, U. Glatzel, and M. Feller-Kniepmeier: *Acta Metall. Mater.*, 1996, vol. 44, pp. 1967-77.
23. R. Völkl, U. Glatzel, and M. Feller-Kniepmeier: *Scripta Metall. Mater.*, 1994, vol. 31, pp. 1481-86.
24. P. Caron, T. Khan, and Y.G. Nakagawa: *Scripta Metall.*, 1986, vol. 20, pp. 499-502.
25. G.E. Dieter: *Mechanical Metallurgy*, 3rd ed., McGraw-Hill Book Co., New York, NY, 1986, pp. 132-35.
26. S.M. Copley and B.H. Kear: *Trans. TMS-AIME*, 1967, vol. 239, pp. 977-84.
27. S.M. Copley and B.H. Kear: *Trans. TMS-AIME*, 1967, vol. 239, pp. 984-92.
28. A. Guimier and J.L. Strudel: *Proc. 2nd Int. Conf. on the Strength of Metals & Alloys, ASM*, Metals Park, Ott, 1970, vol. 3, pp. 1145-49.
29. O.H. Kriege and J.M. Baris: *Trans. ASM*, 1969, vol. 62, pp. 195-200.
30. L. Delehouzee and A. Deruyttere: *Acta Metall.*, 1967, vol. 15, pp. 727-34.
31. B.E.P. Beeston, I.L. Dillamore, and R.E. Smallman: *Met. Sci. J.*, 1968, vol. 2, pp. 12-14.
32. X.S. Xie, G.L. Chen, P.J. McHugh, and J.K. Tien: *Scripta Metall.*, 1982, vol. 16, pp. 484-88.
33. W.F. Hosford: *The Mechanics of Crystals and Textured Polycrystals*, Oxford University Press, Oxford, United Kingdom, 1993, pp. 169-72.
34. P. Caron and T. Khan: *Mater. Sci. Eng.*, 1983, vol. 61, pp. 173-84.
35. T.H. Blewitt, R.R. Coltman, and J.K. Redman: *J. Appl. Phys.*, 1957, vol. 28, pp. 651-60.